ACCOUNTS of chemical research

Article

pubs.acs.org/accounts

Hybrid Perovskites for Photovoltaics: Charge-Carrier Recombination, Diffusion, and Radiative Efficiencies

Published as part of the Accounts of Chemical Research special issue "Lead Halide Perovskites for Solar Energy Conversion".

Michael B. Johnston and Laura M. Herz*

Department of Physics, Clarendon Laboratory, University of Oxford, Parks Road, Oxford OX1 3PU, U.K.

CONSPECTUS: Photovoltaic (PV) devices that harvest the energy provided by the sun have great potential as renewable energy sources, yet uptake has been hampered by the increased cost of solar electricity compared with fossil fuels. Hybrid metal halide perovskites have recently emerged as low-cost active materials in PV cells with power conversion efficiencies now exceeding 20%. Rapid progress has been achieved over only a few years through improvements in materials processing and device design. In addition, hybrid perovskites appear to be good light emitters under certain conditions, raising the prospect of applications in low-cost light-emitting diodes and lasers.

Further optimization of such hybrid perovskite devices now needs to be supported by a better understanding of how light is converted into electrical currents and vice versa. This Account provides an overview of charge-carrier recombination and mobility mechanisms encountered in such materials. Optical-pump−terahertz-probe (OPTP) photoconductivity spectroscopy is an ideal tool here, because it allows the dynamics of mobile charge carriers inside the perovskite to be monitored following excitation with a short laser pulse whose photon energy falls into the range of the solar spectrum.

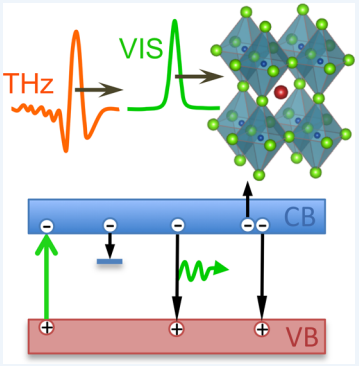

We first review our insights gained from transient OPTP and photoluminescence spectroscopy on the mechanisms dominating charge-carrier recombination in these materials. We discuss that mono-molecular charge-recombination predominantly originates from trapping of charges, with trap depths being relatively shallow (tens of millielectronvolts) for hybrid lead iodide perovskites. Bimolecular recombination arises from direct band-to-band electron−hole recombination and is found to be in significant violation of the simple Langevin model. Auger recombination exhibits links with electronic band structure, in accordance with its requirement for energy and momentum conservation for all charges involved. We further discuss charge-carrier mobility values extracted from OPTP measurements and their dependence on perovskite composition and morphology.

The significance of the reviewed charge-carrier recombination and mobility parameters is subsequently evaluated in terms of the charge-carrier diffusion lengths and radiative efficiencies that may be obtained for such hybrid perovskites. We particularly focus on calculating such quantities in the limit of ultra-low trap-related recombination, which has not yet been demonstrated but could be reached through further advances in material processing. We find that for thin films of hybrid lead iodide perovskites with typical charge-carrier mobilities of ∼30cm^2/(V s), charge-carrier diffusion lengths at solar (AM1.5) irradiation are unlikely to exceed ∼10 μm even if all trap-related recombination is eliminated. We further examine the radiative efficiency for hybrid lead halide perovskite films and show that if high efficiencies are to be obtained for intermediate charge-carrier densities ($n \approx 10^{14}$ cm^{-3}) trap-related recombination lifetimes will have to be enhanced well into the microsecond range.

INTRODUCTION

A new generation of thin-film photovoltaic cells based on hybrid organic−inorganic metal halide perovskite absorbers has recently emerged, exhibiting high efficiencies now exceeding 20% for lead-based compounds.[1] Perovskites are materials that crystallize in the same structure as calcium titanium oxide, that is ABX_3. Here, A is typically an organic cation, such as methylammonium (MA) or formamidinium (FA), B is a divalent metal (Pb, Sn, Ge), and X is a halide anion such as I, Br, or Cl.[2] Such hybrid perovskites allow low-cost solution processing in air and absorb broadly across the solar spectrum, making them an exciting new component for clean energy generation. In addition, photovoltaics devices based on simple thin-film planar-heterojunction architectures are possible[3] for materials with charge-carrier diffusion pathways that are sufficiently long to allow for charge migration through a whole absorber layer.[4] The charge-carrier generation, diffusion, and recombination of free charge carriers are hence crucial to the operation of solar cells, yet an understanding of these properties is only just emerging.

Spectroscopy with radiation in the terahertz frequency range is a powerful tool allowing the examination of charge carriers because their presence significantly modifies the dielectric

Received: September 7, 2015
Published: December 10, 2015

DOI: 10.1021/acs.accounts.5b00411
Acc. Chem. Res. 2016, 49, 146−154

response of a medium in the low-frequency range. Optical-pump−terahertz-probe (OPTP) spectroscopy offers the additional capacity to time-resolve changes in the electric field amplitude ($\Delta T/T$) of a single-cycle terahertz pulse transmitted through a sample as a function of time delay after optical excitation (see Figure 1). For photoconductive materials, the recorded transients typically reflect changes in photoconductivity, $\sigma = en\mu$, where e is the elementary charge, n the photoinduced charge-carrier density, and μ the charge-carrier mobility.[5] Therefore, with knowledge of the absorbed photon density and the photon-to-charge branching ratio ϕ, the charge-carrier mobility can be extracted from the initial values of $\Delta T/T$ in a contactless fashion.[5] The subsequent decay of the photoconductivity signal is generally attributed to charge-carrier dynamics, such as recombination or transfer across interfaces.[5,6] OPTP offers time resolution only limited by the (sub-picosecond) pulse durations and allows the full amplitude waveform of the terahertz pulse to be recorded, from which the time-depdendent complex photoconductivity spectrum in the terahertz region can be extracted, allowing an analysis of the conduction mechanisms. We have previously used OPTP to examine photovoltaic materials such as polymer−fullerene blends[7] and dye-sensitized mesoporous metal-oxide layers, unravelling, for exammple, the mechanisms underlying light-soaking effects,[8] delayed electron injection,[6,9] charge trapping,[10] and interface engineering.[11,12] Therefore, hybrid metal-halide perovskites provided an ideal opportunity for us to establish the photophysics that make these materials so highly effective as light absorbers and charge conductors.

CHARGE-CARRIER RECOMBINATION MECHANISMS

Figure 1a shows the terahertz photoconductivity transients[5] recorded for a thin film of $MAPbI_{3-x}Cl_x$ produced via dual-source vapor deposition as described in ref 3. These decay dynamics are typical for thin films of hybrid lead iodide perovskites produced through a number of different fabrication techniques and film architectures.[5,13−15] At high excitation pulse fluences (corresponding to high initial charge-carrier densities) charge-carrier dynamics are fast, indicating recombination processes involving more than one charge-carrier, such as bimolecular electron−hole or Auger recombination. At very low fluences, the photoconductivity signal plateaus over the 2.5 ns observation window, showing that density-independent, monomolecular recombination is associated with significantly longer lifetimes. In hybrid lead halide perovskites such monomolecular recombination channels are therefore typically assessed through simpler techniques that do not require sub-picosecond time resolution, such as time-correlated single photon counting (TCSCP).[5,16] Figure 1b shows a typical time-resolved photoluminescence (PL) transient for the same $MAPbI_{3-x}Cl_x$ film, as recorded by TCSPC. At low excitation fluence, decay tails become monoexponential in accordance with monomolecular decay channels.

The dynamics of charge-carrier recombination through monomolecular and higher-order processes are generally governed by the following rate equation

$$\frac{dn}{dt} = G - k_1 n - k_2 n^2 - k_3 n^3 = G - nR_T(n) \quad (1)$$

where G is the charge-density generation rate, k_1 the monomolecular charge-recombination rate, k_2 the bimolecular electron−hole recombination rate constant, and k_3 the Auger recombination rate constant. Here $R_T(n)$ is the total charge recombination rate given by

$$R_T = k_1 + nk_2 + n^2 k_3 \quad (2)$$

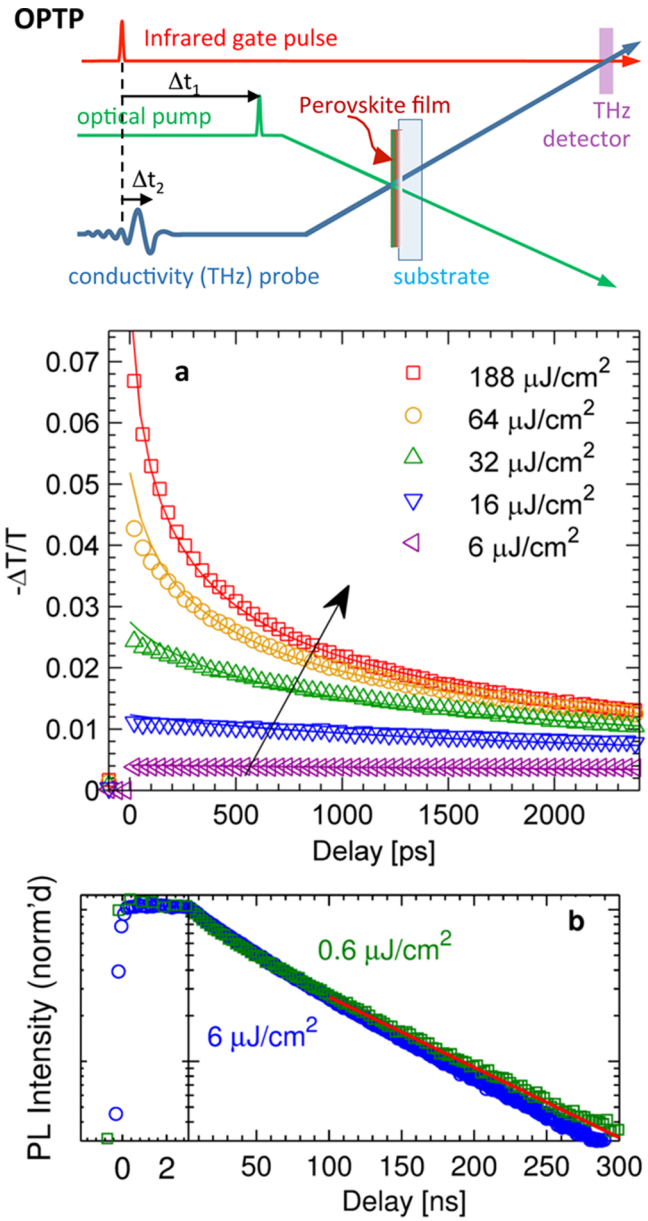

Figure 1. (top) Schematic representation of pulsed laser beam lay-out for the optical-pump−terahertz-probe (OPTP) technique. (bottom) Charge-carrier recombination dynamics for a thin film of dual-source vapor-deposited $MAPbI_{3-x}Cl_x$ following pulsed excitation with photons of energy above the band gap. (a) Photoinduced terahertz conductivity transients monitored over a 2.5 ns window following pulsed (50 fs) excitation at 550 nm (2.25 eV) with a range of pulse fluences. With increasing fluence, bimolecular and Auger recombination lead to increasingly rapid initial decay components. Reproduced from ref 5 with permission from The Royal Society of Chemistry. (b) Photoluminescence decay transients measured over a 300 ns window following pulsed (200 ps) excitation at 633 nm (1.96 eV). In this low fluence regime, charge-carrier recombination dynamics are mostly monoexponential and independent of excitation fluence, indicating the dominance of trap-assisted (monomolecular) recombination. Reprinted with permission from ref 17. Copyright 2014 American Chemical Society.

DOI: 10.1021/acs.accounts.5b00411
Acc. Chem. Res. 2016, 49, 146−154

Table 1. Summary of Charge-Carrier Mobility and Recombination Parameters for Different Hybrid Metal Halide Perovskites

perovskite[a]	deposition method[b]	film architecture[c]	charge-carrier mobility[d] [cm^2 (V s)$^{-1}$]	recombination constants			refs
				k_1[e] [s^{-1}]	k_2[f] [cm^3 s^{-1}]	k_3[g] [cm^6 s^{-1}]	
$MAPbI_{3-x}Cl_x$	solution	meso Al_2O_3	12	5×10^6	0.9×10^{-10}	1.0×10^{-28}	13
$MAPbI_{3-x}Cl_x$	2-source vapor	flat film	33	12×10^6	1.1×10^{-10}	0.2×10^{-28}	5, 17
$MAPbI_3$	solution	meso Al_2O_3	8	14×10^6	9.2×10^{-10}	1.3×10^{-28}	13
$MAPbI_3$	solution	flat film	35	15×10^6	0.6×10^{-10}	1.6×10^{-28}	15
$FAPbI_3$	solution	flat film	27	7×10^6	1.1×10^{-10}	0.2×10^{-28}	14
$FAPbBr_3$	solution	flat film	14	21×10^6	11×10^{-10}	1.5×10^{-28}	14
$MASnI_3$	solution	meso TiO_2	1.6	8×10^9	14×10^{-10}		18

[a]Chemical formulae, where MA is CH_3NH_3 (methylammonium) and FA is $HC(NH_2)_2$ (formamidinium). [b]Through a solution precursor or via dual-source vapor deposition under vacuum. [c]Perovskite flat films or infusions into a mesoporous metal oxide matrix. [d]Charge-carrier mobility at terahertz frequencies. [e]Monomolecular rate constant. [f]Bimolecular rate constant. [g]Auger rate constant.

which depends on charge-carrier density n and, for pulsed excitation, time t. Global fitting of the solutions to eq 1 to data such as those shown in Figure 1 allows for the extraction of k_1, k_2, and k_3 for any examined material. Through this method, we have extracted such rate constants for a wide range of hybrid metal halide perovskites,[5,13−15,18] as summarized in Table 1. Below we review our findings on rates and mechanisms associated with these three contributing recombination pathways.

Monomolecular charge-carrier recombination is by definition a process involving one "particle", which in a typical semiconductor may constitute either a conduction-band electron, a valence-band hole, or an exciton composed of an already bound electron−hole pair. The current consensus view is that the predominant species present at room temperature in hybrid lead halide perovskites are free charges rather than excitons.[2] This notion is supported by the relatively low values of the exciton binding energy reported at room-temperature for these materials[19−21] and by observations of just one characteristic recombination kinetic, independent of whether photoluminescence, transient absorption, or photoconductivity are probed.[4,13,22] Therefore, the monomolecular decay component observed for these materials most likely originates from trap-assisted recombination, which depends on the trap cross-section, energetic depth, density, and distribution, which are subject to sample processing and handling conditions.

Table 1 shows example values obtained for samples fabricated at Oxford, ranging between $k_1 = 5 \times 10^6$ and 21×10^6 s^{-1} ($\tau \approx 50$−200 ns) for hybrid lead halide perovskites but a much wider spectrum of values (ranging between $k_1 = 1 \times 10^6$ and 250×10^6 s^{-1}) has been reported[2,4,21−24] across the literature in accordance with widely differing processing protocols. For $MASnI_3$ on the other hand, we reported a monomolecular recombination rate that was almost 3 orders of magnitude higher than those typical for $MAPbI_3$ (see Table 1). We have attributed this effect to high self-doping of $MASnI_3$ in the presence of Sn^{4+}, which leads to fast recombination of electrons with a high background density of holes released from such p-dopants.[18] For the mixed-halide iodide−bromide perovskite system $FAPb(Br_yI_{1-y})_3$, we have shown the monomolecular recombination rate to be strongly linked with crystalline disorder.[14] For thin-film materials within the central region ($y \approx 0.3$−0.5), trap-related recombination was found to be significantly accelerated,[14] in correlation with compositional instabilities and amorphous morphologies that occur in this region.[25] These examples highlight the expected correlation of trap-related recombination with material purity and crystallinity.

To gain further insight into the nature and mechanisms of trapping in hybrid perovskites, we have recently examined the trap-mediated recombination rate k_1 for $MAPbI_3$ over the temperature range of 8−340 K.[15] Values for k_1 were found to decrease monotonically with decreasing temperature across all three crystal phases probed. Such a temperature dependence is consistent with charge trapping by ionized impurities: as the temperature is lowered, donated dopant charges return to the ionized impurities, in effect passivating them.[15] From an Arrhenius analysis, the activation energy for such trap passivation was found to be 20 meV in the room-temperature tetragonal phase of $MAPbI_3$ films,[15] in agreement with other experimental[23] and theoretical[26,27] studies suggesting the presence of predominantly shallow traps in $MAPbI_3$.

Bimolecular charge-carrier recombination between electrons and holes in a direct semiconductor can be viewed as intrinsic photon-radiative recombination that directly relates to the reverse process of light absorption. Bimolecular recombination rate constants k_2 therefore ought to exhibit significantly lower dependence on material processing than trap-assisted charge recombination. Table 1 displays bimolecular recombination rate constants that we determined using OPTP for a range of hybrid metal halide perovskites with different film architectures. Values range between 0.6×10^{-10} and 14×10^{-10} cm^3 s^{-1} at room temperature,[5,13−15,18] which is comparable with the bimolecular recombination rate constant of $\sim 4 \times 10^{-10}$ cm^3 s^{-1} for the direct inorganic semiconductor GaAs.[28] Table 1 shows that some variation exists in the extracted value of k_2 even for similar materials, which may for example arise from infusion of the material into a mesoporous metal-oxide scaffold that may affect crystallite size[24] and the value of the dielectric function of the effective medium[29] comprising a nanostructured metal-oxide/perovskite composite. While comparisons therefore have to be made with care, the values shown in Table 1 suggest that lighter halides and metals yield higher bimolecular recombination rates. For example, k_2 appears to be substantially larger[18] for $MASnI_3$ than the equivalent lead-containing compound $MAPbI_3$. Similarly, we have recently shown[14] that across the mixed-halide iodide−bromide perovskite system $FAPb(Br_yI_{1-y})_3$, the bimolecular recombination rate constant increases monotonically with increasing bromide content y by an order of magnitude from $FAPbI_3$ to $FAPbBr_3$. One possibility is that such effects are linked to bandstructure modifications, for example, through changes in spin−orbit coupling that have been shown to be sizable in such materials.[30] For the comparison of bromide with iodide lead perovskites, in particular, the well-known enhancement in excitonic binding energy for the bromide perovskites[31] may in addition lead to

DOI: 10.1021/acs.accounts.5b00411
Acc. Chem. Res. 2016, 49, 146−154

changes in the continuum absorption near the band edge that can potentially contribute to the observed[14] increase in bimolecular recombination. A correlation of such bimolecular recombination rates with appropriate theoretical models would be highly desirable because it may aid the design of suitable new hybrid perovskite materials.

Materials with relatively low charge-carrier mobility are often referenced against the simple Langevin model, which assumes that recombination will occur once an electron and a hole move within their joint capture radius, which is presumed to be larger than their mean free path.[32] The Langevin model thus proposes a correlation between the bimolecular recombination rate constant k_2 and the charge-carrier mobility μ according to $k_2/\mu = e/(\epsilon_0\epsilon_r)$ because the charge-capture rate is enhanced through an increase in the approach velocity between electrons and holes. In an early study, we showed that the ratio of the bimolecular recombination constants k_2 of $MAPbI_3$ and $MAPbI_{3-x}Cl_x$ to the charge-carrier mobility was lower by at least 4 orders of magnitude than that stipulated by the Langevin model.[13] We have since examined all materials listed in Table 1 and found similarly strong deviations from the simple Langevin theory.[5,14,15,18] Materials whose ratio of k_2/μ falls short of the Langevin limit are highly desirable for photovoltaic applications, because they allow for long charge-carrier diffusion lengths, L_D. We have shown[5] that if bimolecular rate constants adhered to the prediction of Langevin theory, $L_D \approx 100$ nm would be expected for $MAPbI_{3-x}Cl_x$ (as opposed to an actual value of 3 μm) at solar irradiation levels. Therefore, the non-Langevin bimolecular recombination in hybrid metal halide perovskites is crucial for photovoltaic devices with planar heterojunction architecture.

Non-Langevin bimolecular recombination has often served as a benchmark for photovoltaic materials with low charge-carrier mobility, for example, as in demixed blends of conjugated polymers with fullerene derivatives[7] or amorphous silicon.[33] For these materials, non-Langevin behavior was attributed to a spatial charge separation between electrons and holes. We have proposed[13] that similar effects may arise in hybrid lead-iodide perovskites because their valence band maxima consist of 6s- and 5p-orbitals of lead and iodine, while conduction band minima mostly incorporate 6p-orbitals of lead.[30,31] Therefore, a weak preferential localization of electrons and holes in different regions of the perovskite unit cell may cause a reduction in the spatial overlap of electron and hole wave functions and hence recombination rates.[13] Such "self-trapping" effects of conduction-band electrons or valence-band holes in different atomic vicinities have been postulated for a range of metal halide crystals some decades ago[34] and will generally lead to strong electron−phonon coupling or polaronic effects.[34] We note that Stokes shifts between absorption onset and photoluminescence emission peaks are at most of the order of several millielectronvolts for $MAPbI_3$ at room temperature[15] suggesting that polaronic shifts are relatively small. However, we have demonstrated that terahertz photoconductivity spectra of $MAPbI_3$ carry modulations from lead-halide vibrations suggesting coupling between photoinduced charge-carriers and phonon modes.[5,15] In addition, we showed the line width of the room-temperature emission from $MAPbI_{3-x}Cl_x$ films to be mostly homogeneously broadened with a broadening mechanisms arising from electron-phonon coupling.[17] Therefore, while polaronic or "self-trapping" effects in $MAPbI_3$ seem to be small compared with some metal-halide crystals, general electron−phonon coupling appears to have an effect on charge-carrier dynamics and recombination that requires further investigation into its nature and strength.

As an alternative approach, bimolecular radiative recombination in hybrid metal halide perovskites may be considered solely through the principle of detailed balance, taking into account the absorption and refractive index functions that arise from the electronic bandstructure near the band edge.[21,35] Such approaches have been highly successful in modeling radiative recombination in high-charge-mobility inorganic semiconductors such as GaAs from band structure parameters.[36]

An analysis of the temperature-dependence of k_2 allows further insight into the mechanisms for bimolecular charge recombination. We have recently conducted temperature-dependent OPTP measurements[15] on thin films of $MAPbI_3$ to determine k_2 in the range between 8 and 360 K. We reported a substantial increase in k_2 with decreasing temperature, across the three crystal phases. This effect may on the one hand be conceptually understood in the context of the simple Langevin model because we also observe a strong increase in charge-carrier mobility with decreasing temperature.[15] Hence, the approach velocity into the joint Coulomb potential of the electron and hole may be increased with decreasing temperature, enhancing bimolecular recombination. Again, an alternative and perhaps quantitatively more suitable explanation may be provided through an evaluation of changes in band-to-band recombination with temperature. For GaAs, the bimolecular recombination rate constant has been shown[37] to increase with decreasing temperature T according to $k_2 \approx T^{-1.5}$, which agreed well with bandstructure calculations within the Kane model for III−V semiconductors.[36] Similarly, analytical expressions for band-to-band recombination in two-dimensional semiconductors are able to correctly reflect the T^{-1} increase in bimolecular recombination with decreasing temperature.[38] In this band-structure picture, the temperature dependence of the bimolecular recombination derives to a large extent from the changes in thermal occupation of the electron−hole states near the band edge.

Auger recombination of charge-carriers is a many-body process involving recombination of an electron with a hole, accompanied by energy and momentum transfer to a further electron or a hole.[39] As a result, Auger recombination is strongly dependent on charge-carrier density as described by the Auger rate constant k_3 in eq 1. Auger recombination must conserve energy and momentum and therefore strongly depends on electronic band structure.[40] Simultaneous energy and wavevector conservation tends to be difficult to achieve when only two bands (e.g., a conduction and a valence band) are involved. Efficient Auger recombination therefore often includes additional bands, such as split-off bands arising from spin−orbit coupling, and may be aided by phonons accepting or donating momentum.[40]

Table 1 summarizes Auger recombination constants that we obtained from OPTP for hybrid lead-halide perovskites with different organic cations, halides, and film architectures.[5,13−15] We found a relatively narrow range of values ($k_3 = (0.2-1.6) \times 10^{-28}$ cm^6 s^{-1}), which is on average ~25 times higher than the Auger rate constant for GaAs.[28] High-charge-density applications such as lasers may therefore suffer higher nonradiative Auger losses when based on hybrid lead-halide perovskites. However, we have recently shown that the expected strong link between Auger rates and crystal structure does appear to hold for such perovskites,[14,15] and hence suitable band structure engineering may well reduce these rates dramatically. For

DOI: 10.1021/acs.accounts.5b00411
Acc. Chem. Res. 2016, 49, 146−154

example, we demonstrated that Auger rate constants in $MAPbI_3$ exhibit exceptionally strong structural phase specificity, falling with increasing temperature in the orthorhombic phase (8−160 K), rising in the tetragonal phase (160−315 K), and falling again as the temperature is raised above 315 K in the cubic phase.[15] In addition, we found[14] that the Auger rate constant for the mixed iodide−bromide perovskite system $FAPb(Br_yI_{1-y})_3$ increased monotonously by an order of magnitude when the bromide fraction y was increased from 0 to 1, which coincides with the occurrence of gradual changes in pseudocubic lattice parameter.[25] Given the high flexibility of the perovskite lattice, further compositional changes that reduce Auger rates may well be feasible. Currently, hybrid perovskites are mostly developed for photovoltaic applications for which Auger recombination bears relatively little importance. For the emerging research on perovskite lasers,[41−44] a somewhat different focus on bandstructure engineering for reduced Auger rates may be an interesting avenue for future work.

CHARGE-CARRIER MOBILITY AND DIFFUSION LENGTHS

Based on initial photoconductivity values measured with OPTP, we have determined the effective charge-carrier mobility, $\phi\mu$, for a range of hybrid metal halide perovskites,[5,13−15,18] as shown in Table 1. We note that these values represent the summation over hole and electron mobilities because both contribute to the photoconductivity response. As discussed above, at room temperature bound excitons are a minority species in these materials, and we therefore assume that these values reflect the actual charge-carrier mobility values, μ.

Table 1 shows that terahertz mobility values for flat films of $MAPbI_3$, $MAPbI_{3-x}Cl_x$, and $FAPbI_3$ are all near 30 cm^2 $(V\ s)^{-1}$. Values for lead halide perovskites infused into mesoporous metal oxide matrices, on the other hand, are somewhat lower (8−12 cm^2 $(V\ s)^{-1}$) in accordance with smaller grain sizes and interfaces that may limit charge motion. Interestingly, we have shown that the photoconductivity spectra for high-quality hybrid lead halide perovskite films across the terahertz frequency range are compatible with a standard Drude free-carrier response in the low-frequency limit; that is, they exhibit a flat, positive real part of the conductivity and a near-zero imaginary part.[5,14,15] For the tin alternative $MASnI_3$ on the other hand, we have observed the real and imaginary parts of the photoconductivity to increase with terahertz frequency, in accordance with charge-localization effects[18] similar to what is typically found for mesoporous metal oxide semiconductors.[11] The low charge-carrier mobility of 1.6 cm^2 $(V\ s)^{-1}$ that we determined for $MASnI_3$ may therefore reflect scattering from impurities and crystal boundaries, rather than the inherent potential of this material. For $MAPbI_3$ and related compounds, the Drude-like conductivity spectra however suggest that substantial enhancements of room-temperature charge-carrier mobilities (e.g., by many orders of magnitude) beyond the value of ∼30 cm^2 $(V\ s)^{-1}$ are unlikely to be achievable. Further evidence for this may be garnered from the temperature dependence of the charge-carrier mobility. We have recently used OPTP to determine $\phi\mu$ for films of $MAPbI_3$ as a function of temperature T and found it to increase with $T^{-1.5}$ from ∼15 cm^2 $(V\ s)^{-1}$ at 370 K to ∼150 cm^2 $(V\ s)^{-1}$at 80 K.[15] Similar temperature dependencies have also been observed for the photoconductivity response of this material in the microwave-frequency range[23] and are typical of charge-carrier mobilities only limited by scattering off phonons,[45] as often observed for inorganic crystalline semiconductors such as silicon[46] and GaAs[47] in the higher-temperature regime. The room-temperature mobility of ∼30 cm^2 $(V\ s)^{-1}$ that we determined for $MAPbI_3$ in the low-frequency regime therefore appears to mostly reflect intrinsic band-transport properties linked with scattering off lattice modes, rather than extrinsic factors such as impurities or grain sizes. We note that average mobilities determined for DC transport over large lengths scales may however still be more significantly limited by grain boundaries and hence be subject to material processing conditions.

Since we are able to determine both charge-carrier mobility and charge-density dependent recombination rates, R_T (see eq 2), from such spectroscopic methods, the charge-carrier diffusion length, L_D, can be evaluated, using

$$L_D(n) = \left(\frac{\mu k_B T}{eR_T(n)}\right)^{1/2} \quad (3)$$

where T is temperature, k_B the Boltzmann constant, and e the elementary charge. Importantly, charge-diffusion lengths need to exceed the typical absorption depths of up to a few hundred nanometers[17] in order for charges to be collected efficiently in planar-heterojunction devices.

Figure 2 shows the room-temperature charge-carrier diffusion length for a typical high-quality hybrid lead iodide perovskite film as a function of charge-carrier density n for a

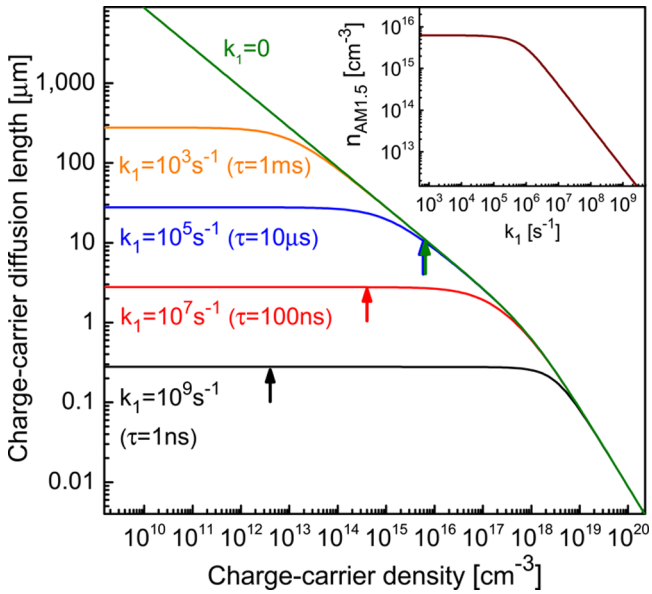

Figure 2. Calculated charge-carrier diffusion lengths, L_D, for hybrid lead iodide perovskite as a function of charge-carrier density for a range of different monomolecular (trap-induced) recombination rates, $k_1 = \tau^{-1}$. Calculations are based on a charge-carrier mobility of 30 cm^2 $(V\ s)^{-1}$, a bimolecular rate constant $k_2 = 10^{-10}$ $cm^3\ s^{-1}$, and an Auger rate constant $k_3 = 10^{-28}$ $cm^6\ s^{-1}$, as typical values for high-quality $MAPbI_3$ (see Table 1). For other values of μ, the displayed L_D has to be multiplied by $[\mu/30\ cm^2\ (V\ s)^{-1}]^{0.5}$. The inset shows, as a function of k_1, the value $n_{AM1.5}$ of the charge-carrier density obtained under steady-state solar (AM1.5) illumination conditions in the absence of charge extraction. The arrows in the main figure indicate the diffusion lengths that can be obtained at the values of $n_{AM1.5}$ for the given trap-related recombination rates; that is, they mark diffusion lengths attainable under AM1.5 in the absence of charge extraction.

DOI: 10.1021/acs.accounts.5b00411
Acc. Chem. Res. 2016, 49, 146−154

range of different values of the monomolecular (trap-assisted) charge-carrier recombination rate. In accordance with Table 1, we here assume the following values: μ = 30 cm^2 (V s)$^{-1}$, k_2 = 10^{-10} cm^3 s^{-1} and k_3 = 10^{-28} cm^6 s^{-1}. For a monomolecular lifetime of $\tau \approx 100$ ns ($k_1 \approx 10^7$ s^{-1}) typical of standard $MAPbI_3$ films, charge-carrier diffusion lengths approach 3 μm in the low-charge-density regime, as we have previously reported.[5,15]

Given that the recombination parameters k_2 and k_3 are mostly intrinsic to the material (as discussed above), we are able to further make predictions on diffusion lengths that may be attainable if extrinsic, trap-assisted recombination rates (k_1) are to be varied, for example, through processing routes. Figure 2 shows that as k_1 approaches zero, the diffusion length becomes strongly dependent on n even in the low charge-carrier density regime, approaching the relationship L_D = 0.88 μm × (10^{18} cm^{-3}/n)$^{1/2}$ for $MAPbI_3$ as $n \ll 10^{18}$ cm^{-3}. Therefore, in the regime of ultralow trap densities in particular, any charge-carrier diffusion length stated can only be sensibly provided within the context of the charge-carrier density present.

The inherent dependence of the charge-diffusion length on charge-carrier density raises the question of how these results relate to a typical photovoltaic device setting. An accurate answer would require full modeling of device characteristics, including charge-carrier drift under perceived electric fields, which is beyond this Account. However, as a simple indicative approach, we consider flat-band conditions close to V_{OC} during which little current density is extracted. In this case, we may approximate $dn/dt = 0$ in eq 1 and solve the resulting cubic equation under knowledge of the spatially averaged generation rate $\langle G \rangle$ under AM1.5 solar illumination conditions to obtain a representative steady-state charge-carrier density, $n_{AM1.5}$. Here we again take k_2 = 10^{-10} cm^3 s^{-1} and k_3 = 10^{-28} cm^6 s^{-1} as typical values for hybrid lead halide perovskite. To determine $\langle G \rangle$, we evaluate the charge-density generation profile along the film depth z according to $G(z) = (hc)^{-1} \int f_{solar}(\lambda)\alpha(\lambda) \exp(-\alpha(\lambda)z)\lambda \, d\lambda$ and extract an average value $\langle G \rangle = 4 \times 10^{21}$ cm^{-3} s^{-1} for a typical film thickness of 300 nm. Here $\alpha(\lambda)$ is the absorption coefficient for a typical hybrid lead iodide film taken from ref 17, and f_{solar} is the ASTM G173-03 Global Tilt reference spectrum for the solar spectral irradiance distribution, with $\int f_{solar}(\lambda) \, d\lambda$ = 1 kW/m^2.

The inset of Figure 2 shows the value of $n_{AM1.5}$ as a function of the monomolecular charge recombination rate k_1. For the range of ultralow k_1 = 0–10^5 s^{-1} (corresponding to $\tau = k_1^{-1}$ = 10 μs to ∞), we find that $n_{AM1.5} \approx 6 \times 10^{15}$ cm^{-3} because bimolecular recombination is the dominant pathway here. For higher values of k_1, however, trap-mediated recombination becomes the dominant process, yielding $n_{AM1.5} = \langle G \rangle \tau$ (where $\tau = k_1^{-1}$), for example, $n_{AM1.5} \approx 4 \times 10^{14}$ cm^{-3} for τ = 100 ns. These values are indicated by corresponding vertical arrows in Figure 2 pointing to the typical charge-carrier diffusion lengths to be expected for different trap-related recombination rates under solar illumination and non-charge-extracting conditions. We note that under such conditions, a charge-carrier diffusion length of ~10 μm will not be exceeded for μ = 30 cm^2 (V s)$^{-1}$ even if all trap-related recombination is eliminated. The diffusion length scales with the square root of the charge-carrier mobility, and therefore values of L_D for different assumed charge-carrier mobilities μ can simply be obtained by multiplication of the y-axis labels in Figure 2 by (μ/[30 cm^2 (V s)$^{-1}$])$^{1/2}$. Hence to reach a diffusion length of, for example, 175 μm under flat-band solar illumination conditions, the mobility would have to increase 300-fold over the value of 30 cm^2 (V s)$^{-1}$ assumed here, that is, to ~9200 cm^2 (V s)$^{-1}$ even in the complete absence of trap-mediated charge recombination. It is therefore unlikely that such elevated charge-carrier diffusion lengths can be reached under actual solar illumination conditions.

RADIATIVE EFFICIENCIES

The distinction of charge-recombination rates into the three mechanisms discussed above also allows us to evaluate the radiative efficiency of hybrid perovskites, if the radiative contributions from each process are known. Such knowledge is particularly important for an assessment of charge-carrier densities at which light-emitting applications such as LEDs and lasers may operate. Here, the general expectation would be for trap-related recombination (k_1) to be nonradiative because no clear spectral emission signature of trap states has yet been identified at room temperature for hybrid lead halide perovskites. In contrast, electron–hole band-to-band recombination (k_2) in a direct semiconductor ought to be radiative. Finally, Auger recombination (k_3) is inherently nonradiative given that energy and momentum is used for intra- or interband transitions and will mostly be lost. These assignments are supported, for example, by the experimentally observed sharp onsets of PL intensity toward the bimolecular recombination regime[21,22] and an investigation of diode ideality factors that confirmed that while trap-assisted recombination was mainly nonradiative, bimolecular recombination was mostly radiative.[48] Therefore, under these assumptions, the radiative efficiency or photoluminescence quantum yield, Φ, is given by the ratio of radiative to total recombination rate components listed in eq 2, yielding

$$\Phi(n) = \frac{nk_2}{k_1 + nk_2 + n^2k_3} \tag{4}$$

Figure 3 displays Φ as a function of n for different values of the trap-mediated recombination rate k_1, based on bimolecular and Auger rate constants, k_2 = 10^{-10} cm^3 s^{-1} and k_3 = 10^{-28} cm^6 s^{-1} as typical values for hybrid lead iodide perovskites (see Table 1). As expected, Figure 3 demonstrates that with increasing charge-carrier density, Φ initially increases toward the regime of increasing bimolecular recombination but then decreases again as the Auger recombination regime is entered. An examination of eq 4 reveals that the radiative efficiency reaches a maximum value of $\Phi_{max} = (1 + 2\sqrt{k_1k_3/k_2^2})^{-1}$ at the charge-carrier density $n_{peak} = \sqrt{k_1/k_3}$, both of which significantly depend on the trap-mediated recombination rate k_1 (see Figure 4). Light emission from these materials therefore ought to be particularly effective for this "sweet spot" in charge-carrier density at which the bimolecular recombination rate k_2n dominates over both monomolecular (k_1) and Auger (k_3n^2) rates. Comparison with literature reports on the charge-carrier density dependence of Φ suggests that this simple model is surprisingly effective.[21] In addition, we note that onsets of amplified spontaneous emission (ASE) have been reported to occur at excitation pulse fluences of 7–70 μJ cm^{-2} in thin films of $MAPbI_3$, corresponding to peak charge-carrier densities of (1–10) × 10^{18} cm^{-3} for the given scenarios.[41−43] These onset charge densities coincide with the range of high radiative efficiencies for materials with trap-related recombination lifetimes of 10 ns

DOI: 10.1021/acs.accounts.5b00411
Acc. Chem. Res. 2016, 49, 146–154

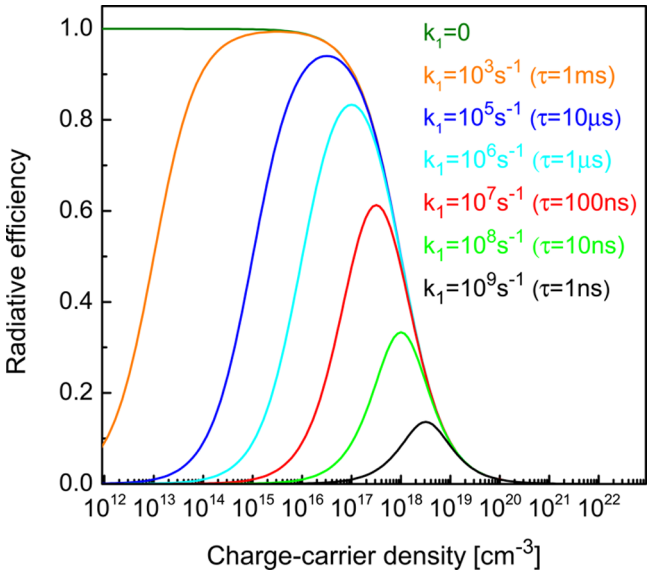

Figure 3. Calculated radiative efficiencies for hybrid lead iodide perovskite as a function of charge-carrier density for a range of different monomolecular (trap-induced) recombination rates, $k_1 = \tau^{-1}$. Calculations are based on the assumption that only bimolecular recombination (here with a typical rate constant $k_2 = 10^{-10}$ cm^3 s^{-1}) contributes to radiative emission, while Auger recombination ($k_3 = 10^{-28}$ cm^6 s^{-1}) and monomolecular recombination are solely nonradiative.

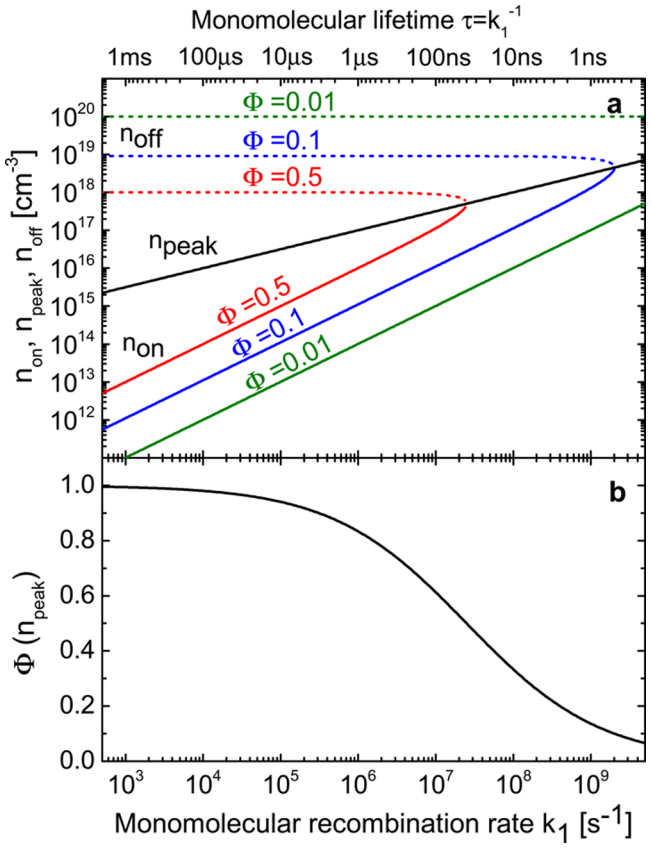

Figure 4. (a) Charge-carrier densities at which radiative efficiencies, Φ, reach 0.01 (1%), 0.1 (10%), 0.5 (50%), or peak values for $MAPbI_3$, plotted as a function of monomolecular recombination rate k_1. The top axis shows the corresponding monomolecular lifetime $\tau = k_1^{-1}$, which is the monoexponential lifetime exhibited in the low-fluence excitation regime; n_{on} (n_{off}) is the charge carrier density below (above) the efficiency peak at which the stated value of Φ is reached, and n_{peak} is the charge-carrier density at which maximum Φ is reached. (b) Maximum value of the radiative efficiency, Φ, reached at the charge-carrier density n_{peak}. Calculations are based on the assumption that only bimolecular recombination (with $k_2 = 10^{-10}$ cm^3 s^{-1}) contributes to radiative emission, while Auger recombination ($k_3 = 10^{-28}$ cm^6 s^{-1}) and monomolecular recombination are solely nonradiative.

to a few hundred nanoseconds, which are typical values now routinely achieved for these materials. Our trends shown in Figure 3 demonstrate that a significant reduction in trap-related recombination may allow for much-reduced onsets of efficient light-emission and ASE in these materials. To allow for quantitative targets, we plot in Figure 4a, as a function of the trap-related monomolecular recombination rate k_1, the charge-carrier densities n_{on} and n_{off} at which values of 50%, 10%, and 1% radiative efficiency are reached. These curves show that for light-emitting devices to operate efficiently even in the medium charge-density regime (~10^{14} cm^{-3}), trap-related recombination lifetimes will have to be in the microsecond regime.

CONCLUSIONS AND OUTLOOK

Hybrid metal halide perovskites have shown impressive performance as light harvesters and are emerging as promising light emitters. We have shown that their success is based on highly favorable charge-carrier mobility and recombination parameters. Charge-carrier mobilities are orders of magnitude above what would be expected from their ratio with bimolecular recombination rate constants from Langevin theory. As a result, both effective light absorption and charge conduction are possible, which makes these materials ideal for photovoltaic applications. High charge-carrier diffusion lengths in the range of 1−10 μm are achievable at solar irradiation levels even for currently typical monomolecular, trap-related recombination rates of tens to hundreds of nanoseconds. As a result, highly efficient solar cells based on planar-heterojunction architectures are already a reality at present. Our analysis shows that efficient operation of light-emitting applications based on these materials will require significant further reduction in trap-related recombination rates. However, these current boundaries could be changed dramatically through further research into new processing protocols that reduce trap densities and by judicious material band structure design to tune bimolecular and Auger recombination rates. Hence our assessment of intrinsic optoelectronic parameters of hybrid metal hybrid perovskites suggests a bright future for this material class.

AUTHOR INFORMATION

Corresponding Author

*E-mail: laura.herz@physics.ox.ac.uk.

Funding

The authors thank the EPSRC for financial support.

Notes

The authors declare no competing financial interest.

Biographies

Michael Johnston received his Ph.D. in Physics from the University of New South Wales in 2000. He is currently a Professor of Physics at the University of Oxford.

DOI: 10.1021/acs.accounts.5b00411
Acc. Chem. Res. 2016, 49, 146−154

Laura Herz received her Ph.D. in Physics from the University of Cambridge in 2002. She is currently a Professor of Physics at the University of Oxford.

REFERENCES

(1) Green, M. A.; Emery, K.; Hishikawa, Y.; Warta, W.; Dunlop, E. D. Solar cell efficiency tables (Version 45). *Prog. Photovoltaics* **2015**, *23*, 1−5.

(2) Herz, L. M. Charge carrier dynamics in organic-inorganic metal halide perovskites. *Annu. Rev. Phys. Chem.* **2016**, DOI: 10.1146/annurev-physchem-040215-112222.

(3) Liu, M.; Johnston, M. B.; Snaith, H. J. Efficient Planar Heterojunction Perovskite Solar Cells by Vapour Deposition. *Nature* **2013**, *501*, 395−398.

(4) Stranks, S. D.; Eperon, G. E.; Grancini, G.; Menelaou, C.; Alcocer, M. J. P.; Leijtens, T.; Herz, L. M.; Petrozza, A.; Snaith, H. J. Electron-Hole Diffusion Lengths Exceeding 1 Micrometer in an Organometal Trihalide Perovskite Absorber. *Science* **2013**, *342*, 341−344.

(5) Wehrenfennig, C.; Liu, M.; Snaith, H. J.; Johnston, M. B.; Herz, L. M. Charge-Carrier Dynamics in Vapour-Deposited Films of the Organolead Halide Perovskite $CH_3NH_3PbI_{3-x}Cl_x$. *Energy Environ. Sci.* **2014**, *7*, 2269−2275.

(6) Tiwana, P.; Docampo, P.; Johnston, M. B.; Snaith, H. J.; Herz, L. M. Electron Mobility and Injection Dynamics in Mesoporous ZnO, SnO_2, and TiO_2 Films Used in Dye-Sensitized Solar Cells. *ACS Nano* **2011**, *5*, 5158−5166.

(7) Parkinson, P.; Lloyd-Hughes, J.; Johnston, M. B.; Herz, L. M. Efficient generation of charges via below-gap photoexcitation of polymer-fullerene blend films investigated by terahertz spectroscopy. *Phys. Rev. B: Condens. Matter Mater. Phys.* **2008**, *78*, 115321.

(8) Tiwana, P.; Docampo, P.; Johnston, M. B.; Herz, L.; Snaith, H. The origin of an efficiency improving "light soaking" effect in SnO_2 based solid-state dye-sensitized solar cells. *Energy Environ. Sci.* **2012**, *5*, 9566−9573.

(9) Raavi, S. S. K.; Docampo, P.; Wehrenfennig, C.; Alcocer, M. J. P.; Sadoughi, G.; Herz, L. M.; Snaith, H. J.; Petrozza, A. The Impact of Molecular Charge-Transfer States on Photocurrent Generation in Solid State DSSCs Employing Low Band-Gap Dyes. *J. Phys. Chem. C* **2014**, *118*, 16825−16830.

(10) Wehrenfennig, C.; Palumbiny, C. M.; Snaith, H. J.; Johnston, M. B.; Schmidt-Mende, L.; Herz, L. M. Fast Charge-Carrier Trapping in TiO_2 Nanotubes. *J. Phys. Chem. C* **2015**, *119*, 9159−9168.

(11) Tiwana, P.; Parkinson, P.; Johnston, M. B.; Snaith, H. J.; Herz, L. M. Ultrafast Terahertz Conductivity Dynamics in Mesoporous TiO_2: Influence of Dye Sensitization and Surface Treatment in Solid-State Dye-Sensitized Solar Cells. *J. Phys. Chem. C* **2010**, *114*, 1365−1371.

(12) Docampo, P.; Tiwana, P.; Sakai, N.; Miura, H.; Herz, L.; Murakami, T.; Snaith, H. J. Unraveling the Function of an MgO Interlayer in Both Electrolyte and Solid-State SnO_2 Based Dye-Sensitized Solar Cells. *J. Phys. Chem. C* **2012**, *116*, 22840−22846.

(13) Wehrenfennig, C.; Eperon, G. E.; Johnston, M. B.; Snaith, H. J.; Herz, L. M. High Charge Carrier Mobilities and Lifetimes in Organo Lead Trihalide Perovskites. *Adv. Mater.* **2014**, *26*, 1584−1589.

(14) Rehman, W.; Milot, R. L.; Eperon, G. E.; Wehrenfennig, C.; Boland, J. L.; Snaith, H. L.; Johnston, M. B.; Herz, L. M. Charge-carrier dynamics and mobilities in formamidinium lead mixed-halide perovskites. *Adv. Mater.* **2015**, DOI: 10.1002/adma.201502969.

(15) Milot, R. L.; Eperon, G. E.; Snaith, H. J.; Johnston, M. B.; Herz, L. M. Temperature-dependent charge-carrier dynamics in $CH_3NH_3PbI_3$. *Adv. Funct. Mater.* **2015**, *25*, 6218−6227.

(16) Wehrenfennig, C.; Liu, M.; Snaith, H. J.; Johnston, M. B.; Herz, L. M. Charge Carrier Recombination Channels in the Low-Temperature Phase of Organic-Inorganic Lead Halide Perovskite Thin Films. *APL Mater.* **2014**, *2*, 081513.

(17) Wehrenfennig, C.; Liu, M.; Snaith, H. J.; Johnston, M. B.; Herz, L. M. Homogeneous Emission Line Broadening in the Organo Lead Halide Perovskite $CH_3NH_3PbI_{3-x}Cl_x$. *J. Phys. Chem. Lett.* **2014**, *5*, 1300−1306.

(18) Noel, N. K.; Stranks, S. D.; Abate, A.; Wehrenfennig, C.; Guarnera, S.; Haghighirad, A. A.; Sadhanal, A.; Eperon, G. E.; Pathak, S. K.; Johnston, M. B.; Petrozza, A.; Herz, L. M.; Snaith, H. J. Lead-Free Organic-Inorganic Tin Halide Perovskites for Photovoltaic Applications. *Energy Environ. Sci.* **2014**, *7*, 3061−3068.

(19) Even, J.; Pedesseau, L.; Katan, C. Analysis of multivalley and multibandgap absorption and enhancement of free carriers related to exciton screening in hybrid perovskites. *J. Phys. Chem. C* **2014**, *118*, 11566−11572.

(20) D'Innocenzo, V.; Grancini, G.; Alcocer, M. J.; Kandada, A. R. S.; Stranks, S. D.; Lee, M. M.; Lanzani, G.; Snaith, H. J.; Petrozza, A. Excitons versus free charges in organo-lead tri-halide perovskites. *Nat. Commun.* **2014**, *5*, 3586.

(21) Saba, M.; Cadelano, M.; Marongiu, D.; Chen, F.; Sarritzu, V.; Sestu, N.; Figus, C.; Aresti, M.; Piras, R.; Geddo Lehmann, A.; Cannas, C.; Musinu, A.; Quochi, F.; Mura, A.; Bongiovanni, G. Correlated electron-hole plasma in organometal perovskites. *Nat. Commun.* **2014**, *5*, 5049.

(22) Yamada, Y.; Nakamura, T.; Endo, M.; Wakamiya, A.; Kanemitsu, Y. Photocarrier recombination dynamics in perovskite $CH_3NH_3PbI_3$ for solar cell applications. *J. Am. Chem. Soc.* **2014**, *136*, 11610−11613.

(23) Oga, H.; Saeki, A.; Ogomi, Y.; Hayase, S.; Seki, S. Improved understanding of the electronic and energetic landscapes of perovskite solar cells: high local charge carrier mobility, reduced recombination, and extremely shallow traps. *J. Am. Chem. Soc.* **2014**, *136*, 13818−13825.

(24) D'Innocenzo, V.; Srimath Kandada, A. R.; De Bastiani, M.; Gandini, M.; Petrozza, A. Tuning the light emission properties by band gap engineering in hybrid lead halide perovskite. *J. Am. Chem. Soc.* **2014**, *136*, 17730−17733.

(25) Eperon, G. E.; Stranks, S. D.; Menelaou, C.; Johnston, M. B.; Herz, L. M.; Snaith, H. J. Formamidinium lead trihalide: a broadly tunable perovskite for efficient planar heterojunction solar cells. *Energy Environ. Sci.* **2014**, *7*, 982−988.

(26) Yin, W.-J.; Shi, T.; Yan, Y. Unusual defect physics in $CH_3NH_3PbI_3$ perovskite solar cell absorber. *Appl. Phys. Lett.* **2014**, *104*, 063903.

(27) Kim, J.; Lee, S.-H.; Lee, J. H.; Hong, K.-H. The role of intrinsic defects in methylammonium lead iodide perovskite. *J. Phys. Chem. Lett.* **2014**, *5*, 1312−1317.

(28) Sheik-Bahae, M.; Epstein, R. I. Can Laser Light Cool Semiconductors? *Phys. Rev. Lett.* **2004**, *92*, 247403.

(29) Bruggeman, D. A. G. Berechnung verschiedener physikalischer Konstanten von heterogenen Substanzen. *Ann. Phys.* **1935**, *416*, 636−664.

(30) Even, J.; Pedesseau, L.; Jancu, J.-M.; Katan, C. Importance of spin-orbit coupling in hybrid organic/inorganic perovskites for photovoltaic applications. *J. Phys. Chem. Lett.* **2013**, *4*, 2999−3005.

(31) Tanaka, K.; Takahashi, T.; Ban, T.; Kondo, T.; Uchida, K.; Miura, N. Comparative study on the excitons in lead-halide-based perovskite-type crystals $CH_3NH_3PbBr_3CH_3NH_3PbI_3$. *Solid State Commun.* **2003**, *127*, 619−623.

(32) Langevin, P. The recombination and mobilities of ions in gases. *Ann. Chim. Phys.* **1903**, *28*, 433−530.

(33) Adriaenssens, G. J.; Arkhipov, V. I. Non-Langevin Recombination in Disordered Materials with Random Potential Distributions. *Solid State Commun.* **1997**, *103*, 541−543.

(34) Williams, R. T.; Song, K. S. The self-trapped exciton. *J. Phys. Chem. Solids* **1990**, *51*, 679−716.

(35) van Roosbroeck, W.; Shockley, W. Photon-radiative recombination of electrons and holes in germanium. *Phys. Rev.* **1954**, *94*, 1558−1560.

(36) Stern, F. Gain-current relation for GaAs lasers with n-type and undoped active layers. *IEEE J. Quantum Electron.* **1973**, *9*, 290−294.

(37) 'tHooft, G. W.; van Opdorp, C. Temperature dependence of interface recombination and radiative recombination in (Al,Ga) As heterostructures. *Appl. Phys. Lett.* **1983**, *42*, 813−815.

DOI: 10.1021/acs.accounts.5b00411
Acc. Chem. Res. 2016, 49, 146−154

(38) Matsusue, T.; Sakaki, H. Radiative recombination coefficient of free carriers in GaAs-AlGaAs quantum wells and its dependence on temperature. *Appl. Phys. Lett.* **1987**, *50*, 1429−1431.
(39) Beattie, A. R.; Landsberg, P. T. Auger Effect in Semiconductors. *Proc. R. Soc. London, Ser. A* **1959**, *249*, 16−29.
(40) Haug, A. Auger recombination in direct-gap semiconductors: band-structure effects. *J. Phys. C: Solid State Phys.* **1983**, *16*, 4159−4172.
(41) Xing, G.; Mathews, N.; Lim, S. S.; Yantara, N.; Liu, X.; Sabba, D.; Grätzel, M.; Mhaisalkar, S.; Sum, T. C. Low-temperature solution-processed wavelength-tunable perovskites for lasing. *Nat. Mater.* **2014**, *13*, 476−480.
(42) Chen, K.; Barker, A. J.; Morgan, F. L. C.; Halpert, J. E.; Hodgkiss, J. M. Effect of Carrier Thermalization Dynamics on Light Emission and Amplification in Organometal Halide Perovskites. *J. Phys. Chem. Lett.* **2015**, *6*, 153−158.
(43) Stranks, S. D.; Wood, S. M.; Wojciechowski, K.; Deschler, F.; Saliba, M.; Khandelwal, H.; Patel, J. B.; Elston, S.; Herz, L. M.; Johnston, M. B.; Schenning, A. P.; Debije, M. G.; Riede, M.; Morris, S. M.; Snaith, H. J. Enhanced amplified spontaneous emission in perovskites using a flexible cholesteric liquid crystal reflector. *Nano Lett.* **2015**, *15*, 4935−4941.
(44) Deschler, F.; Price, M.; Pathak, S.; Klintberg, L. E.; Jarausch, D.-D.; Higler, R.; Hüttner, S.; Leijtens, T.; Stranks, S. D.; Snaith, H. J.; Atatüre, M.; Phillips, R. T.; Friend, R. H. High photoluminescecen efficiency and optically pumped lasing in solution-processed mixed halide perovskite semiconductors. *J. Phys. Chem. Lett.* **2014**, *5*, 1421−1426.
(45) Yu, P. Y.; Cardona, M. *Fundamentals of Semiconductors*, 1st ed.; Springer: Berlin, 1996.
(46) Ferry, D. K. First-order optical and intervalley scattering in semiconductors. *Phys. Rev. B* **1976**, *14*, 1605−1609.
(47) Stillman, G. E.; Wolfe, C. M.; Dimmock, J. O. Hall coefficient factor for polar mode scattering in n-type GaAs. *J. Phys. Chem. Solids* **1970**, *31*, 1199−1204.
(48) Wetzelaer, G.-J. A. H.; Scheepers, M.; Sempere, A. M.; Momblona, C.; Avila, J.; Bolink, H. J. Trap-assisted non-radiative recombination in organic-inorganic perovskite solar cells. *Adv. Mater.* **2015**, *27*, 1837−1841.

DOI: 10.1021/acs.accounts.5b00411
Acc. Chem. Res. 2016, 49, 146−154